Study of the correlation between columnar aerosol burden, suspended matter at ground and chemical components in a background European environment

Víctor Estellés,[1] José A. Martínez-Lozano,[1] Jorge Pey,[2] Michaël Sicard,[3,4] Xavier Querol,[2] Anna R. Esteve,[1] María P. Utrillas,[1] Mar Sorribas,[5] Gotzon Gangoiti,[6] Andrés Alastuey,[2] and Francesc Rocadenbosch[3,4]

Received 3 June 2011; revised 9 December 2011; accepted 10 December 2011; published 16 February 2012.

[1] Although routinely monitored by ground based air quality networks, the particulate matter distribution could be eventually better described with remote sensing techniques. However, valid relationships between ground level and columnar ground based quantities should be known beforehand. In this study we have performed a comparison between particulate matter measurements at ground level at different cut sizes (10, 2.5 and 1.0 μm), and the aerosol optical depth obtained by means of a ground based sunphotometer during a multiinstrumental field campaign held in El Arenosillo (Huelva, Spain) from 28 June to 4 July 2006. All the PM fractions were very well correlated with AOD with correlation coefficients that ranged from 0.71 to 0.81 for PM10, PM2.5 and PM1. Furthermore, the influence of the mixing layer height in the correlations was explored. The improvement in the correlation when the vertical distribution is taken into account was significant for days with a homogeneous mixing layer. Moreover, the chemical analysis of the individual size fractions allowed us to study the origin of the particulate matter. Secondary components were the most abundant and also well correlated in the three size fractions; but for PM10 fraction, chemical species related to marine origin were best correlated. Finally, we obtained a relationship between MODIS L3 AOD from collection 5.1 and the three PM cut sizes. In spite of being a relatively clean environment, all the techniques were able to capture similar day to day variations during this field campaign.

Citation: Estellés, V., et al. (2012), Study of the correlation between columnar aerosol burden, suspended matter at ground and chemical components in a background European environment, *J. Geophys. Res.*, *117*, D04201, doi:10.1029/2011JD016356.

1. Introduction

[2] Atmospheric pollution by aerosols is defined as the change in the atmosphere's natural composition due to the suspension of particles, either by natural causes or by the action of man [*Mészáros*, 1999], and is one of the major environmental problems in developed countries [*Lipfert et al.*, 2000; *Pope et al.*, 2002]. The effects of aerosols over human health mostly depend on their size distribution [*World Health Organization*, 1999]. In fact, according to their ability to penetrate in the different areas of the respiratory system, particulate matter is classified in *inhalable* (which can enter the respiratory system), *thoracic* (which can penetrate into the conducting airways and the bronchial region of the lung), and *respirable* (which can enter the deepest part of the lung) [*Wilson*, 1998]. For practical reasons, the aerodynamic diameter thresholds for these types of particles are fixed at 10 μm (PM10), 2.5 μm (PM2.5), and 1 μm (PM1), respectively. National authorities have fixed limits for the emission of particulate matter (PM), first regulating the PM10 levels, and now fixing limits on PM2.5. For example, in USA the EPA (Environmental Protection Agency) regulated the levels of PM2.5 in September 2006 (U.S. Environmental Protection Agency, Standards, 2006, accessed May 2010, http://www.epa.gov/air/particlepollution/standards.html), while in Europe they were regulated in 2008 [*European Parliament*, 2008]. PM1 levels are still not regulated by these legislations, although there are evidences that human health could be even more sensitive to PM1 than PM2.5 and PM10.

[3] In general, particulate matter is measured at ground level by networks of ground based instruments managed by public administrations (generally at regional scale) with the purpose of protecting the public health. The spatial representativity of these networks is low and limited to the specific

[1]Grupo de Radiación Solar, Departamento Física de la Tierra y Termodinámica, Universidad de Valencia, Valencia, Spain.
[2]Instituto de Diagnóstico Ambiental y Estudios del Agua, CSIC, Barcelona, Spain.
[3]Department of Signal Theory and Communications, Universitat Politècnica de Catalunya, Barcelona, Spain.
[4]Institut d'Estudis Espacials de Catalunya, Universitat Politècnica de Catalunya, Barcelona, Spain.
[5]Estación de Sondeos Atmosféricos "El Arenosillo," INTA, Huelva, Spain.
[6]Departamento de Ingeniería Química y del Medio Ambiente, Universidad del País Vasco, Bilbao, Spain.

0148-0227/12/2011JD016356

Table 1. Summary of References Using a CIMEL CE318 Radiometer to Correlate AOD With Ground PM Measurements

Author (Year)	Dominant aerosol	λ (nm)	Time Averages	Correlation Coefficient	Time Period	Ground Measurement	Ground Instrument	Vertical Profiles	Chemical Analysis
Smirnov et al. [2000]	Mineral oceanic	870	Daily and Monthly	0.71–0.93	3 years	Dust concentration	High volumen filters	N/A	Dust mass
Corbin et al. [2002]	Urban	670	Daily	0.42–0.55	95 days	PM2.5, PM10	Filter sample array	N/A	Sulfate, Nitrate, OM, soil
Xia et al. [2006]	Polluted urban	440	Daily (by season)	0.37–0.77	33 months	PM10	TEOM	N/A	N/A
Mukai et al. [2006]	Maritime	870	Daily	0.65	3 months	PM2.5, TSP-PM2.5	SPM-613D	N/A	N/A
Mukai et al. [2007]	Maritime	870	Daily	0.65	3 months	PM2.5	SPM-613D	N/A	N/A
Cheng et al. [2008]	Dust	440	Daily	<0.6	18 days	PM10	PIXIE impactor	N/A	20 trace elements
Schäfer et al. [2008]	Urban	560	Daily (by season)	0.69–0.94 (extinction)	4 + 11 days	PM10, PM2.5, PM1, PM10–PM25	SEQ47/50 Leckel	LIDAR (1064,532, 355 nm)	N/A
Boyouk et al. [2010]	Urban polluted	532	Hourly	0.78–0.85	11 days	PM2.5	TEOM	LIDAR 532 nm	N/A
Schaap et al. [2009]	Rural	-	Daily	0.57–0.64	10 months	PM2.5	TEOM	LIDAR 1064 nm	N/A
Zhang et al. [2010]	Dust	532	Hourly	0.94 (lidar)	3 days	PM10	TEOM	LIDAR 532 nm	N/A

places where measurements are acquired. Moreover, in many cases poor coordination exists between regional networks.

[4] However, atmospheric aerosols can also be measured by remote sensing. This technique allows filling in the gaps between ground level networks due to the broad spatial coverage of satellite imaging, but its accuracy and resolution is still low [*Schaap et al.*, 2009]. Many studies have derived the aerosol burden from satellite remote sensing, especially from the Aqua and Terra satellites which carry on board the MODIS sensor (MODerate-resolution Imaging Spectroradiometer). Correlations between the aerosol optical depth (AOD) obtained by MODIS and the PM measured at ground level have been previously made for different world areas, mainly United States, Europe and China [*Wang and Christopher*, 2003; *Slater et al.*, 2004; *Hutchison et al.*, 2005; *Koelemeijer et al.*, 2006; *van de Kassteele et al.*, 2006; *van Donkelaar et al.*, 2006; *Kaskaoutis et al.*, 2008; *Guo et al.*, 2009; *Tian and Chen*, 2010]. Moreover, *Chu et al.* [2003] used MODIS images to characterize the aerosol load at the North of Italy, the city of Los Angeles and the urban area of Beijing.

[5] Before remote sensing data could be routinely used as a proxy to monitor particulate matter, in situ measurements at ground level must be related to columnar retrievals performed from the ground. Several studies have obtained empirical relationships between the column integrated AOD and PM2.5 and PM10 concentrations for different regions and environments. The AOD was obtained with different instruments, as the Multifilter Rotating Shadowband Radiometer (MFRSR) [*Kim et al.*, 2006]; the LICOR spectroradiometer [*Alföldy et al.*, 2007]; the MICROTOPS Sun photometer [*Das et al.*, 2009]; manually operated Sun photometers [*Ramachandran*, 2005]; Linke-Feussner actinometers [*Veefkind et al.*, 1996] and LIDAR [*Raut and Chazette*, 2009].

[6] Nevertheless, CIMEL sunphotometer is the most employed instrument for characterizing the column integrated AOD. Since year 2000, several articles have employed CIMEL to retrieve the AOD and correlate it with measurements at ground level of total particulate matter [*Smirnov et al.*, 2000], PM10 [*Corbin et al.*, 2002; *Xia et al.*, 2006; *Cheng et al.*, 2008; *Schäfer et al.*, 2008; *Schaap et al.*, 2009; *Zhang et al.*, 2010], PM2.5 [*Corbin et al.*, 2002; *Mukai et al.*, 2006, 2007; *Schäfer et al.*, 2008; *Schaap et al.*, 2009; *Boyouk et al.*, 2010] and PM1 [*Schäfer et al.*, 2008]. In some other articles, LIDAR retrievals were also used to determine the height of the mixing layer [*Schäfer et al.*, 2008; *Schaap et al.*, 2009; *Boyouk et al.*, 2010; *Zhang et al.*, 2010; *Córdoba-Jabonero et al.*, 2011]. Table 1 summarizes the foremost studies focusing on the correlation between ground PM measurements and AOD obtained using CIMEL Sun photometers. Most of these studies use daily PM10 or PM2.5 measurements in different environments (usually urban, maritime or under the influence of high dust loads) and spanning from 3 days to 3 years, mostly from few weeks to few months. Sometimes, chemical parameters have also been introduced, and only recently LIDAR retrievals have been used to check the influence of the mixing layer height (MLH) in the correlation between ground and column retrievals.

[7] One of the objectives of the DAMOCLES (Determinación de Aerosoles por Medidas Obtenidas en Columna, Lidar y Extinción, y Superficie) thematic network created in

Table 2. Summary of DAMOCLES Instruments and Measurements Used in This Study

Type of Aerosol Retrieval	Instrument/Technique	Specifications
In situ sampling	High volume samplers (DIGITEL and MCV)	Particulate matter collection at PM10, PM2.5 and PM1 (12 h resolution)
	Grimm Model 1107	Particle size distribution at 10 min resolution (0.3–10.0 μm)
Chemical analysis	ICP-AES/ICP-MS	~60 major and trace elements and components
	Ionic chromatography	Cl^-, SO_4^{2-}, NO_3^-, NH_4^+
	LECO	Total, Organic and Elemental Carbon
Columnar burden	Cimel CE318	Aerosol optical depth at 500 nm (~15 min resolution)
Vertical profiling	LIDAR	Aerosol optical coefficients and mixing layer height (30 min resolution)
Remote sensing	MODIS (C5.1, level 3)	Aerosol optical depth at 550 nm

2004, was to put together different Spanish groups that independently measure and characterize atmospheric aerosols from different points of view, including its characterization at ground level and at the whole atmospheric column. Keeping this idea in mind, DAMOCLES organized a field campaign during the summer of 2006 in the installations of the INTA (National Institute of Aerospace Technology) in El Arenosillo (Huelva) (37.1°N, 6.7°W, 40 m a.s.l.) to compare different instrumentation for aerosol characterization [*Martínez-Lozano et al.*, 2007]. The campaign took place between 28 June and 4 July of 2006. Due to its location, the sounding station of El Arenosillo is an exceptional site for short-term and long-term determination of atmospheric parameters [*Pey et al.*, 2008; *Sorribas*, 2008].

[8] In this article we study the relationship of the AOD measured by the CIMEL Sun photometers with the PM10, PM2.5 and PM1 measured by different instruments during the DAMOCLES field campaign, including the effect of the mixing layer height estimated from LIDAR profiles. We also include a discussion about the effect of an episode of pollution transported from western Iberia on the chemical composition and vertical distribution of particles.

2. Instrumentation and Methodology

2.1. Instrumentation

[9] In Table 2 we summarize all the instruments and techniques used in this study. For in situ aerosol gravimetric characterization, high volume samplers (DIGITEL and MCV) with DIGITEL cut-off inlets for PM10, PM2.5 and PM1 were deployed. PM10, PM2.5 and PM1 sampling was carried out on quartz fiber filters Schlëicher and Schuell (QF20 150 mm). Quartz fiber filters were first pre-treated at 200°C. Before and after sampling, the filters were conditioned at 20°C and 50% RH, after that these were weighted at least three times to obtain constant values. Mass PM concentrations were determined by difference of weight.

[10] Filters were analyzed by different techniques in order to determinate the levels of about 60 elements and components. A bulk sample acidic (HF:HClO4:HNO3) digestion of 1/2 of each filter and subsequent determination of major and trace elements by means of Inductively Coupled Atomic Emission Spectrometry (ICP-AES) and Inductively Coupled Plasma Mass Spectrometry (ICP-MS). The content of Cl^-, SO_4^{2-} and NO_3^- was obtained by means of ionic chromatography and a selective electrode was used to determine the NH_4^+ concentration. Total carbon (TC) content was measured by using an elemental carbon analyzer (LECO). Levels of organic and elemental carbon (OC and EC) were determined in PM1 samples following the method described by *Pio et al.* [1994]. Following these procedures it was possible to obtain the concentrations of major species (SiO, CO_3^{2-}, Al, Ca, Na, Mg, K, Fe, SO_4^{2-}, NO_3^-, Cl^- and NH_4^+) and trace elements (Li, P, Ti, V, Cr, Mn, Co, Ni, Cu, Zn, As, Se, Rb, Sr, Mo, Cd, Sn, Sb, Ba, La, Ce, Hf, Pb, Bi, Th, U). Details on instruments and analytical procedures are given by *Pey et al.* [2008].

[11] PM10, PM2.5 and PM1 levels were also continuously monitored (on a 10 min basis), using a laser spectrometer GRIMM 1107. This instrument provides real time measurements of number concentrations for PM0.3–10 that are automatically converted to mass concentrations for the three size fractions by applying specific privative algorithms. In order to harmonize the concentration measurements, the resulting PM data were corrected using factors obtained by the comparison with gravimetric measurements performed simultaneously for each fraction. In all cases both measurements showed good agreement, with correlation coefficients R^2 between 0.8 and 0.9. High volume (30 m^3 $hour^{-1}$) instruments MCV-CAV for PM10 and PM2.5 and DIGITEL for PM1, equipped with cut off DIGITEL inlets, were employed to collect PM10, PM2.5 and PM1 fractions. Sampling periods were intended with 12 h resolution, from 10 to 22 h and 22–10 h local time. This sampling program resulted in the collection of 14 valid samples for each fraction.

[12] The columnar aerosol optical depth was retrieved by seven CIMEL CE318 Sun photometers included in the RIMA/AERONET (Red Ibérica de Medida de Aerosoles/AERosol Robotic NETwork) networks [*Cachorro et al.*, 2007] and one independent instrument from the University of Valencia. The CIMEL CE318 is a solar photometer designed for automatic measurements of direct solar irradiance and sky radiance at 440, 500, 670, 870, 940, and 1020 nm channels. The full width at half maximum (FWHM) is some 2–10 nm, depending on the channel. The sensor head is equipped with a double collimator with a 1.2 ° field of view (FOV). *Estellés et al.* [2006, 2010, 2011] described and validated the algorithms used in this study to calculate the AOD from the CE318 radiometer. The comparison (rmsd) of the values obtained this way with the AERONET retrievals was 0.0005–0.0019 for the VIS-NIR channels and 0.0036–0.0051 for the UV channels, well within the associated uncertainty of 0.02.

[13] A total number of five LIDAR instruments were deployed on the site: two laboratory systems from Barcelona and Madrid, a Raymetrics LR321 from Granada, a CIMEL Electronique CAML CE370–2 from Valencia and an Elight UV11 from Cartagena. The LIDARs performed continuous daytime retrievals from 28 June until 2 July. All systems pointed to the zenith. Profiles were acquired with a time resolution of 1 min. The data shown in this paper were acquired with the Barcelona LIDAR system [*Rocadenbosch*

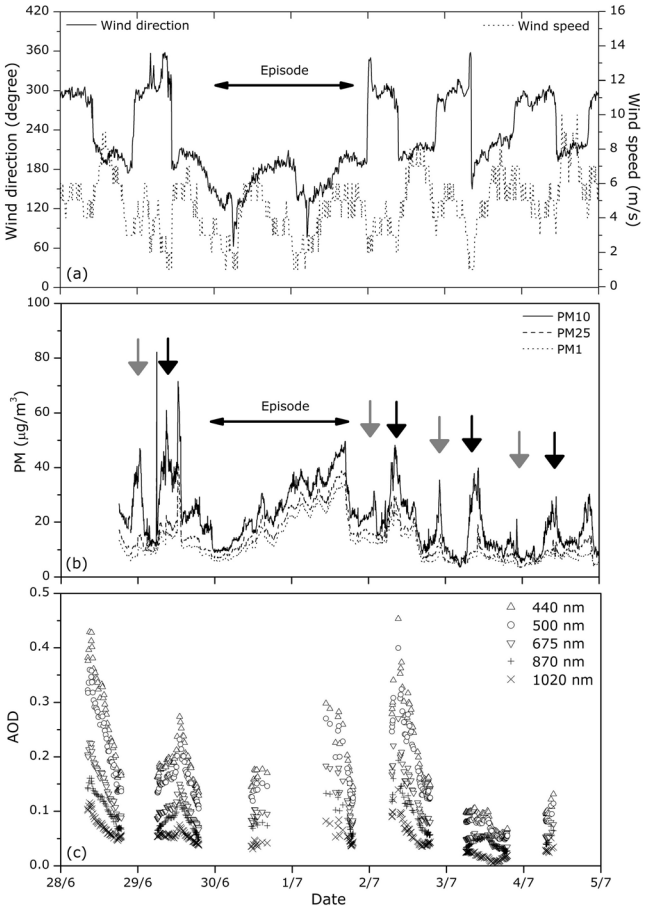

Figure 1. Evolution of (a) wind direction and speed, (b) ground PM levels for 10, 2.5 and 1 μm, and (c) columnar aerosol optical depth, obtained during daytime hours. The anomalous period is framed in the plots. The sea and land breeze onsets are highlighted with black and gray arrows respectively.

et al., 2002] at 532 nm. The aerosol optical coefficient profiles (backscatter and extinction) were retrieved by means of the two-component elastic LIDAR inversion algorithm [*Fernald*, 1984; *Sasano and Nakane*, 1984; *Klett*, 1985] constrained with the Sun photometer-derived AOD [*Reba*, 2010]. The MLH was calculated by means of the gradient method applied to the range-square-corrected signal [*Sicard et al.*, 2006]. This method looks for the absolute negative minimum of the first derivative, which corresponds to the strongest negative gradient of the lidar signal. The mean MLH was calculated with a time resolution of 30 min. All profiles were visually inspected and the resulting MLH was cross-compared to the previous value and the following value in order to guarantee the temporal coherency of its evolution. A description of the LIDAR systems and a comparison of their performances are provided by *Sicard et al.* [2009].

[14] MODIS AOD (collection 5.1) level 3 product from Terra and Aqua platforms has been also used in this study [*Acker and Leptoukh*, 2007]. The data was retrieved as an average value for an area defined by a 1° × 1° square centered on El Arenosillo site for the campaign days.

2.2. Meteorology

[15] During the DAMOCLES 2006 campaign, typical summer conditions prevailed: a thermal low developed over Iberian Peninsula with sunny days but without extremely high temperatures (around 26–28°C during day time and 16–18°C at nighttime), coincident with a long period of Atlantic advections. From now on, three different phases will be identified in the field campaign, based on the analysis of the meteorological synoptic patterns and the atmospheric models simulations [*Pey et al.*, 2008]. During the first phase (from 28 to 29 June) the Azores anticyclone located west of Portugal extended a ridge of high pressures over Western Europe and the British Islands. On the second phase (from 30 June to 1 July) this system was weakened and an eventual particle episode at ground level was detected at the site. This particle event consisted of a long range transport of pollution, detected at ground level by an increase of PM levels, and was described in detail by *Pey et al.* [2008]. During the third phase of the campaign, from 2 July to the end of the field program, a weak low pressure system with its associated front approached to the western coast of Portugal, and forced back to the central Atlantic the higher pressure area of the Azores High, reinforcing again the westerly over the Gulf of Cadiz and at the strait of Gibraltar.

[16] In this synoptic situation, local circulations governed the observed wind regime: day time sea breezes and land-to-sea drainage flows during the night and early morning. As shown in Figure 1a, sea breeze started every day at 11–12 h local time, flowing perpendicular to the coast line (180–190° direction). The land-to-sea flows developed around midnight, and they have generally a 300° direction with a weaker intensity. These observations were in agreement with those obtained in previous studies [*Alastuey et al.*, 2006; *Sánchez de la Campa et al.*, 2007]. However, from 30 June to 1 July the typical northwesterly nighttime regime was replaced by the southeasterlies (120°) flowing almost parallel to the coast, while the daytime sea breeze remained unperturbed. This meteorological event and the absence of nighttime breeze have been highlighted in Figure 1a. Their effect on the PM levels and AOD are presented in Figures 1b and 1c, and will be explained later.

[17] The simulations analyzed by *Pey et al.* [2008] with the mesoscale model Regional Atmospheric Modeling System (RAMS) [*Pielke et al.*, 1992] and HYbrid Particle And Concentration Transport Model (HYPACT) [*Tremback et al.*, 1993] permitted to find the origin of the meteorological episode anomalies: during the episode, a circulation vortex was developed that interrupted the land breeze at nighttime. The arrival of pollution from the Gulf of Cadiz was also found. This simulation of all the possible transport mechanisms operating in the area and the selection of the coast and inland sources accounts for the wide variety of wind regimes of the region.

[18] At a lower resolution, the paths followed by the air masses have been also estimated by their back-trajectories, which allow a broad approximation of the regions with which the air masses had interacted at different levels. One of the most used models for calculating back-trajectories is the Hybrid Single-Particle Lagrangian Integrated Trajectory Model (HYSPLIT) developed by NOAA (R. R. Draxler and G. O. Rolph, HYSPLIT Model, 2003, accessed March 2010

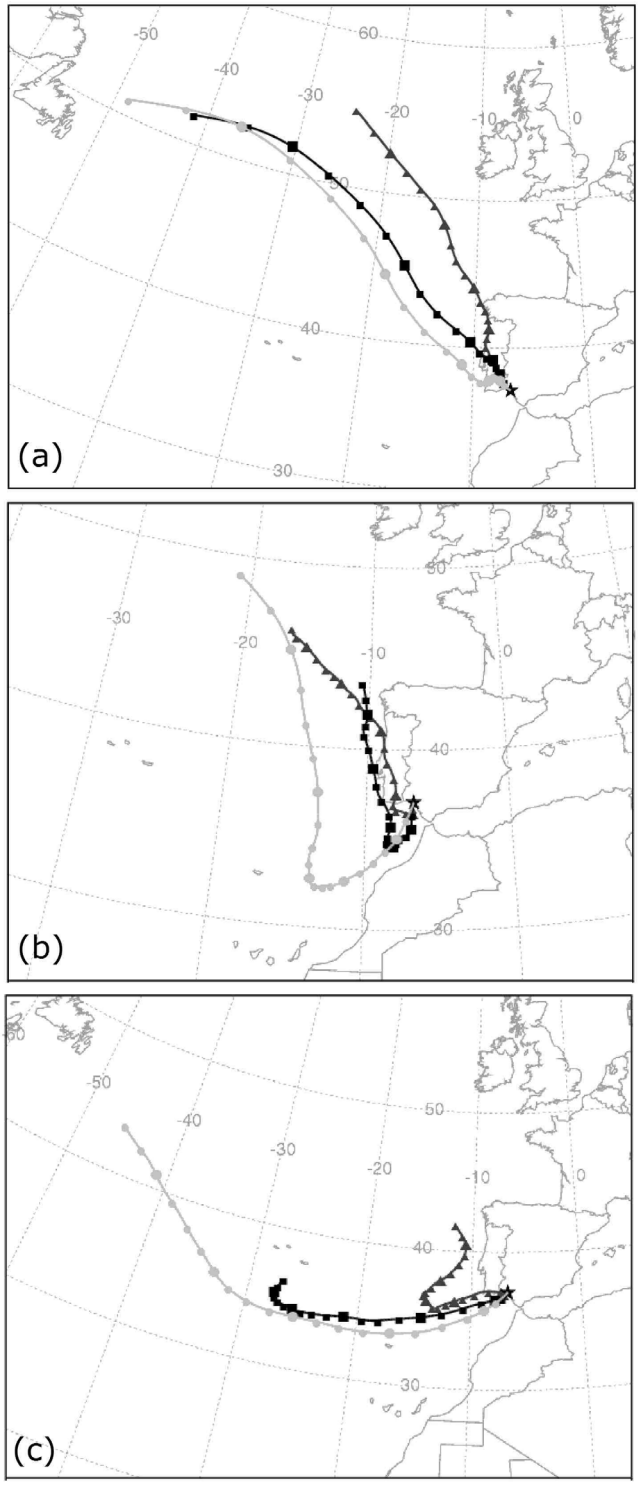

Figure 2. Back-trajectories of air masses arriving at El Arenosillo on (a) 28 June 2006, (b) 1 July 2006, and (c) 3 July 2006. Triangles, squares and circles correspond to 500, 1000 and 1500 m a.g.l. simulations.

via NOAA ARL READY Web site http://www.arl.noaa.gov/ready/hysplit4.html). This model combines a Lagrangian approximation for resolving air mass transport with an Eulerian approximation for the diffusion of pollutants. For each day, back-trajectories were calculated simultaneously starting at different altitudes, based on the LIDAR profiles: (1) 500 m above sea level, well within the boundary layer where the greater part of the interactions affecting the aerosols occur; (2) 1000 m above sea level, usually representing mid to high layers of the boundary layer; and (3) 1500 m above sea level, representative of the top of the boundary layer or bottom of the free troposphere, where some residual layers can still be identified by the LIDAR profiles during the first stage of the field campaign.

[19] In Figure 2, representative back trajectories calculated at 12 h GMT for each of the three stages identified by *Pey et al.* [2008] are shown. During the first phase (28 June) the back trajectories identify the Atlantic northwesterly origin of the air masses. During the meteorological event (1 July) the back trajectories are shorter and slightly more meandering over the arrival area. After the event (3 July) the back trajectories show again an Atlantic air mass origin with no local recirculation, resulting in the cleanest scenario found during the campaign. Although the HYSPLIT back trajectories do not permit to analyze the daily evolution of the air masses to the greater detail of RAMS model, they agree within the different resolutions of the models, already shown by *Pey et al.* [2008].

3. Results and Discussion

3.1. Evolution of AOD, PM Levels and Chemical Composition of PM

[20] The effect of the mid-campaign meteorological episode is evident on the ground PM levels, plotted in Figure 1b. In Figure 1b, evolution of PM10, PM2.5 and PM1 mass concentrations is presented. Peaks on PM are detected at the time of the land and sea breezes onsets, mainly for coarse particles (PM10). These peaks are highlighted in Figure 1b with black and gray arrows for the sea and land breeze onsets, respectively. However, during the meteorological episode the PM levels steadily increased probably due to the nighttime vortex that produced a transport of pollutants from the Gulf of Cadiz and Lisbon area, mixed with nearby emissions. The resultant effect would be the observed steady increase of PM levels at the site. Once the synoptic pattern was restored and the breezes were dominant at the site again, the PM levels recovered their typical daily behavior, as observed during the first days of the field campaign.

[21] The evolution of the columnar aerosol burden, described by the AOD at several wavelengths, is plotted in Figure 1c. Some data is missing in the mornings of days 30 June and 1 July due to the removal of cloudy affected data. Days 28, 29 June and 2 July have a characteristic morning maximum related to the sea breeze circulation; 3 July also has a morning maximum, although sea breeze produces a weaker effect on this columnar load increase. In any case, the values recorded this day both in the column and at ground are very low.

[22] The effect of the aerosol pollution event can be also noticed in the columnar burden. During days 30 June and 1 July, the described daily pattern disappeared. During 30 June, it remains more stable, with minor variations in agreement to PM values recorded at ground. Both PM and AOD values increase from 30 June to 1 July, suddenly decreasing at dusk time when the sea breeze is established,

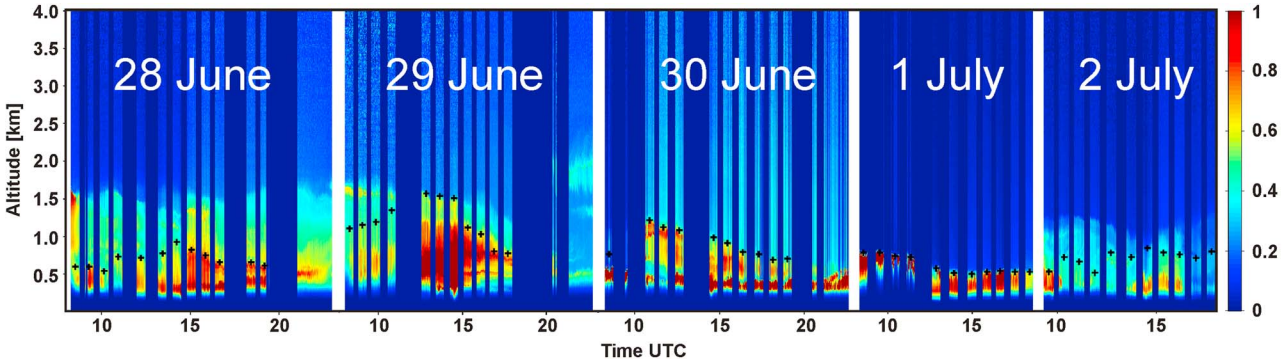

Figure 3. Evolution of the vertical profiles of range-square-corrected LIDAR signal at 532 nm. The color bar represents range-square-corrected LIDAR signal in arbitrary units. The daytime MLH is represented by black plus signs.

blowing from south (180°) and sweeping inland most of the accumulated pollutants.

[23] More insight can be gained if we visually compare the evolution of previous PM and AOD levels with vertical LIDAR profiles. In Figure 3 the evolution of the LIDAR profiles in terms of range-square-corrected signal and the obtained mixing layer height from 28 June to 2 July are plotted. During the first phase of the campaign (days 28 and 29 June) the LIDAR signal profile intensity and the derived MLH had a very good correspondence with AOD and PM levels. The maximum of the MLH is reached between 1200 and 1500 UTC on 29 June around 1.6 km. After 1500 UTC the decrease of the MLH is associated with a decrease of the AOD. In the meantime lofted aerosol layers mostly disappeared. The presence of such layers could be related to residual Saharan dust, progressively removed by the dominant Atlantic advection on 28 June. Measurements at ground were not available until the last part of this day, although a decreasing trend in the three PM sizes is observed from starting measurements. On 29 June the AOD, PM and LIDAR data also showed a good agreement, with maximum values at noon time due to the advection of particles at low levels, and a decreasing trend during the afternoon both in the LIDAR profiles and the aerosol layer height, also detected on ground PM and columnar AOD data.

[24] The aerosol layer was kept relatively confined to the ground during the second phase of the campaign (30 June and 1 July) with very high extinction coefficients within this layer that increased mainly near the ground. The increase on columnar AOD was also detected.

[25] Finally, the mixing layer height was recovered again for the third phase of the campaign (from 2 July). The LIDAR corrected signal reached very low values during the afternoon of 2 July, in agreement with PM and AOD evolution. On 3 July both PM and AOD data showed the lowest daily values of particle concentration and extinction. Unfortunately no LIDAR profile is available for comparison.

[26] A qualitative correlation between ground and columnar retrievals can be therefore deduced by direct comparison of Figures 1b, 1c and 3. Most of the peaks can be identified on the PM and AOD plots, although the minor details are not always in agreement due to evident differences on the vertical distribution of the aerosols. In some cases, changes in concentration at high layers will not have any effect at ground (as expected on the morning of day 28 June). In other occasions, very low and heterogeneous layers of particles could induce strong variations on PM levels, although their total weight on the columnar integrated values could be less important.

[27] The temporal evolution of different chemical elements and components on a daily basis was also investigated.

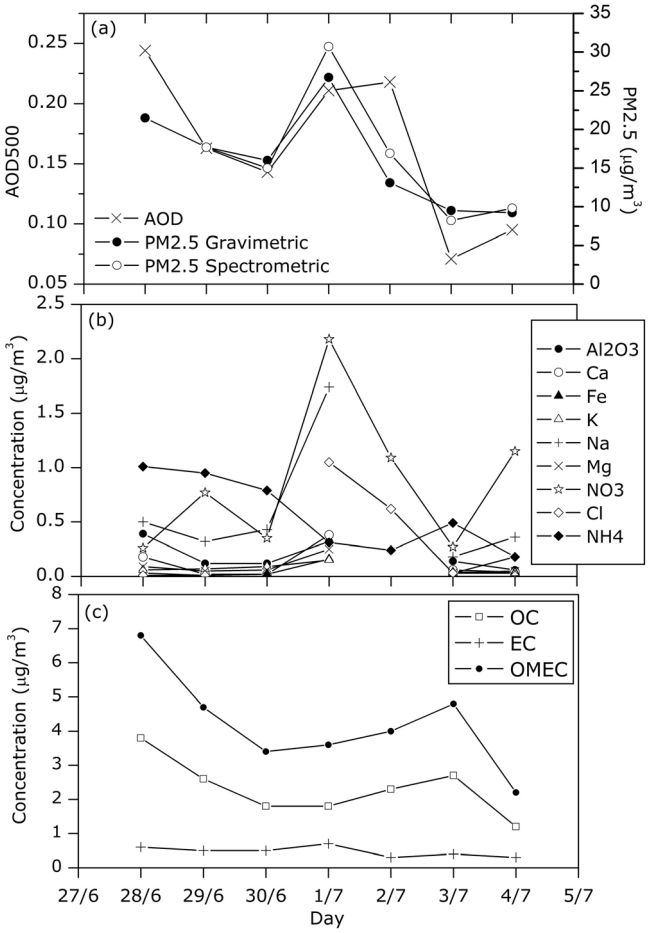

Figure 4. Evolution of (a) 12 h gravimetric and spectrometer PM2.5 levels, compared to daily columnar AOD500; (b) major chemical species; and (c) carbonaceous matter.

Table 3. Correlation Coefficients Obtained by Linear Regression of AOD500 Versus PM10, PM2.5 and PM1 for Instantaneous, Hourly and Daily Values[a]

	PM10	PM2.5	PM1	N
		Daily		
Grav. 24 h	0.91	0.81	0.71	7
Grav. 12 h	0.81	0.75	0.51	7
Grimm 12 h	0.71	0.79	0.78	7
Grimm matched	0.71	0.81	0.80	7
		Hourly		
28	—	—	—	1
29	0.42	0.58	0.63	13
30	0.40	0.41	0.39	7
01	0.60	0.61	0.63	7
02	0.79	0.92	0.93	10
03	0.64	0.39	0.42	13
04	0.85	0.74	0.78	4
Total	0.53	0.75	0.75	55
		Instant		
28	0.05	0.04	0.04	8
29	0.39	0.48	0.55	64
30	0.23	0.33	0.33	11
01	0.59	0.89	0.90	22
02	0.90	0.91	0.92	48
03	0.36	0.30	0.37	67
04	0.75	0.35	0.42	12
Total	0.58	0.76	0.76	232

[a]The number of data points used for the regressions is indicated as N.

In Figure 4a, the gravimetric PM2.5 records are plotted, together with daily GRIMM PM2.5 measurements and also correlated to columnar AOD levels. The 12 h gravimetric levels refer to daytime, it is from 10:00 to 22:00 local time. For the columnar information, the daily mean AOD at 500 nm was selected. In Figure 4a, ground and columnar values follow a similar pattern, with higher levels obtained for the particle episode, mainly day 1 July.

[28] Figures 4b and 4c show the evolution of the major species (Al_2O_3, Ca, Fe, K, Cl, Na, Mg, NO_3 and NH_4^+) and carbonaceous particles (expressed as organic matter + elemental carbon) respectively. Although most major chemical species maximize on 1 July, carbonaceous matter present a different temporal behavior. In fact, during the atmospheric pollution episode their concentration diminished markedly. Only elemental carbon (EC) shows a slight maximum on 1 July. Therefore, the different proportion on carbonaceous matter could be related to the different nature of the local and remote polluted air masses.

3.2. Correlation Between Ground (PM) and Columnar (AOD) Levels

[29] On previous studies (refer to Table 1) comparison of columnar and ground aerosol measurements have been usually performed with filter samplers on a 24 h time basis. During DAMOCLES campaign, filter samplers were operated in a 12 h time basis for day and nighttime periods. Moreover, spectrometers allowed us to monitor the PM levels at a 10 min resolution.

[30] Therefore we first performed linear regressions between AOD at 500 nm and gravimetric PM10, PM2.5 and PM1 levels, using 24 h accumulated levels, only for the sake of comparison with previous references. The correlation coefficients obtained are presented in Table 3 (*Grav. 24 h*). These coefficients were high (0.71–0.91) for the three size fractions, akin to those obtained by *Schäfer et al.* [2008] for an urban ambient (0.7–0.94) during 38 days and similar to those of *Schaap et al.* [2009] (0.61–0.73). Other authors obtained lower correlations for a variety of dominant aerosols and different size of databases. *Zhang et al.* [2010] obtained the highest correlation (0.94) for hourly averages, but it was limited to three days dominated by mineral dust. Despite the good correlation found in our case, the intercept of the regression was slightly negative for PM10.

[31] Correlation coefficients when using 12 h samples were lower (0.5–0.8) with the highest value correspondent to PM10 (see *Grav. 12 h* row in Table 3). The intercept (not shown in Table 3) was still negative for this fraction. The correlation was still good for PM2.5 fraction (0.75) with an intercept of 0.04. *Smirnov et al.* [2000] obtained an intercept of 0.04 when correlating AOD at 870 nm with total dust mass for monthly averages, due in part to aerosols in the free troposphere. In general, we could expect positive intercepts in ground–columnar correlations as occasional high level layers with a high concentration of aerosols would bias the fitting toward positive intercepts.

[32] Gravimetric and spectrometric PM levels corresponded well [*Pey et al.*, 2008]. Due to the higher temporal resolution, from now on the spectrometer measurements will be employed instead to analyze the correlation between AOD500 and PM. To check the effect of using GRIMM instead of gravimetric levels, first we accumulated GRIMM values for 12 h to match the gravimetric sampling time; the resultant correlation coefficients are included in Table 3 for comparison (*Grimm 12 h*). This time, the results were satisfying: (1) the correlation was again high for the three fractions (0.71–0.79); (2) the correlation was highest for PM2.5 and lowest for PM10; and (3) the three intercepts were positive, ranging from ~0.04 for PM1.0 to almost 0 for PM10 (not shown in Table 3). These three characteristics were in agreement with most of the authors that analyzed PM10 and PM2.5 correlations (Table 1).

[33] However, the previous 12 h accumulated values were not representative of the time period when AOD was measured. Thus we performed new correlations by matching both CIMEL and GRIMM sampling times. It is, in the computation of the accumulated values, we only took into account the PM measurements that were acquired during the time when the AOD could be retrieved (daytime, cloudless sky). The results are presented in Table 3 (*Grimm matched*) and represented in Figure 5 (black dots). The correlation coefficient did not change for PM10 (0.71) although it was slightly higher for PM2.5 and PM1 (0.81 and 0.80). The slope was slightly higher (although not significantly) for PM1 (0.007 ± 0.002) than PM2.5 (0.006 ± 0.002) and PM10 (0.005 ± 0.002). The intercepts were 0.06 ± 0.03, 0.05 ± 0.03 and 0.02 ± 0.06 for PM1, PM2.5 and PM10 respectively. These correlation coefficients are lower than those found for 24 h gravimetric mass levels, but give more sensitive results and they are still similar or higher than most of the references in Table 1.

[34] Additional linear fittings have been applied to hourly and instantaneous PM and AOD data. The correlation coefficients have been also included on Table 3. When the hourly fittings are performed day-by-day, the results varied between 0.39 for day 3 July (AOD was relatively stable) and 0.92 for

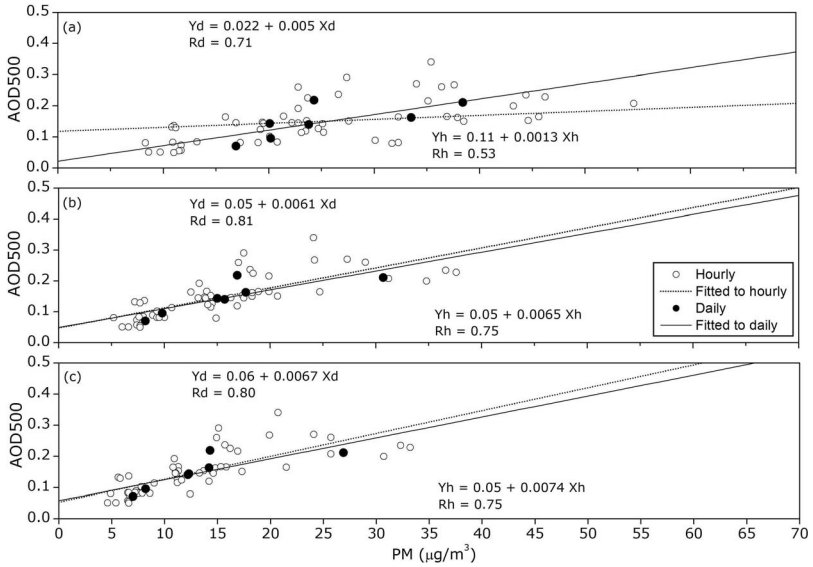

Figure 5. Scatterplot of hourly and daily mean AOD500 versus (a) PM10, (b) PM2.5 and (c) PM1.0. The linear regressions parameters are shown in the plots. Sub indexes 'h' and 'd' refer to hourly and daily fittings.

day 2 July (a clear breeze pattern on AOD). Day 28 was not taken into account because of the low temporal sampling match. For the whole campaign data set, the correlation was 0.53, 0.75 and 0.75 for PM10, PM2.5 and PM1. In Figure 5 we have also included the scatterplots and linear fittings for the hourly data.

[35] For instantaneous measurements, the day-by-day correlations were still lower, although when the whole campaign data set was analyzed, the results were very consistent, with correlation coefficients about 0.58, 0.76 and 0.76 for PM10, PM2.5 and PM1 (Table 3). In all cases, the intercept was positive and the slope was always higher for PM1 and PM2.5 than PM10. Summarizing, when comparing ground and columnar loads, best correlations are obtained when daily averages are used.

3.3. Relationship Between AOD and PM Fractions

[36] In the previous section we have shown that the correlation for AOD versus PM is generally higher for PM2.5 than PM10. In order to better isolate the effect of the different sizes, we have also considered the differences between PM fractions: PM2.5–10 and PM1–2.5. PM2.5–10 would correspond to the so-called coarse mode. PM1–2.5 would correspond to a mid size interval, located between fine and coarse modes. The fine mode referred would be better represented by PM1 fraction.

[37] In Figure 6 the difference PM2.5–10 has been plotted in the abscissa axis. It seems clear that for the dominant air mass during the field campaign, the coarse mode by itself does not drive the previous correlation between ground and columnar levels, as the correlation coefficient is very low (R = 0.11 and 0.14 for daily and hourly averages). The difference PM1–2.5 does not show consistent results when switching from hourly to daily averages. Finally, the fine fraction (PM1) has the highest correlation coefficient (R = 0.80 and 0.75 for daily and hourly averages, as shown in Figure 5) and therefore it could be considered the dominant PM fraction when relating ground and columnar burdens, being responsible to the high correlations obtained for the accumulated PM10 and PM2.5 fractions, at least during this field campaign.

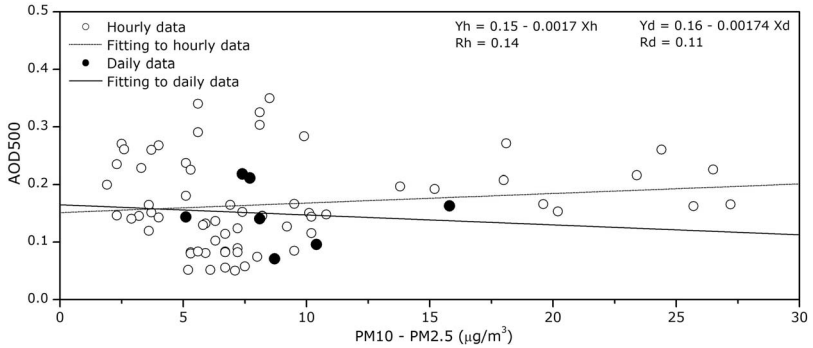

Figure 6. Scatterplot of hourly and daily mean AOD500 versus PM10–PM2.5. The linear regression parameters are shown in the plot.

Table 4. Correlation Coefficients Obtained for the Day by Day Fittings Between Hourly PM Levels and AOD at 500 nm or Derived Extinction Coefficients[a]

	AOD500			β_e (km^{-1})			
Day	PM10	PM2.5	PM1	PM10	PM2.5	PM1	N
28	—	—	—	—	—	—	1
29	0.20	0.47	0.53	0.20	0.13	0.17	11
30	0.40	0.41	0.39	0.46	0.44	0.40	7
01	0.58	0.61	0.63	0.93	0.94	0.95	7
02	0.92	0.92	0.93	0.95	0.94	0.93	10
Total	0.29	0.53	0.57	0.27	0.58	0.62	36

[a]The total represents a fitting through all the hourly points. Day 28 June data point is included in the total fitting, but cannot be fitted separately.

3.4. Influence of the MLH on the Correlation Between AOD and PM

[38] It is well known that the vertical structure is an important factor affecting the relationship between the columnar burden and the ground concentration of particles [*Schaap et al.*, 2009; *Boyouk et al.*, 2010]. To explore the influence of the vertical distribution of aerosols in the correlation, we have used the MLH derived from the LIDAR profiles.

[39] The MLH evolution from 28 June to 2 July was shown in Figure 3. It is apparent that the MLH increases during the morning and decreases during the evening. This daily pattern could be explained by the swelling of the lowest atmospheric layers due to intense insolation of ground.

[40] In order to introduce the effect of the MLH in the correlations, we have followed the approach previously used by other authors such as *Schäfer et al.* [2008]. In particular, the integrated AOD can be related to the vertical distribution of the extinction coefficient by:

$$AOD = \int_0^\infty \beta_e(z)dz \tag{1}$$

where β_e is the extinction coefficient obtained by the LIDAR. Now, the same quantity can be calculated only for the aerosols inside the mixing layer. Let us call AOD_{ML} the AOD integrated between ground and the MLH. If we suppose that the aerosols within the mixing layer are well mixed, then the measurement at ground would be representative of the mixing layer. In this situation we could write:

$$AOD_{ML} = \int_0^{z_B} \beta_e(0)dz = \beta_e(0)z_B \tag{2}$$

In this equation, z_B is the height of the mixing layer. As a consequence, we can estimate a ground level extinction coefficient from the AOD obtained with the sunphotometer and the MLH retrieved from the LIDAR profiles. Once the extinction coefficient has been derived this way, we can correlate it with ground level PM levels.

[41] A summary of the correlation coefficients obtained when using the derived $\beta_e(0)$ instead of AOD have been presented in Table 4. In Table 4, the correlations have been performed day by day. It is worth noting that taking into account the MLH made (1) grow the results worse for 29 June, (2) improve insignificantly for days 30 June and 2 July, and (3) improve very significantly for 1 July. Day 28 data could not be fitted alone because it only included one matching measurement.

[42] The explanation for such a different behavior most probably resides in the multilayer complexity. In these cases, the aerosols are not well mixed and the columnar AOD is not representative of ground measurements. On the contrary, the aerosols are more confined to ground on 1 July, with a well mixed layer most of the time. This could explain such an improvement on the daily correlation (0.61 to 0.94, in the case of PM2.5).

[43] If we compute the correlation using all hourly data from 30 June to 2 July, the correlation would improve from 0.57 to 0.69 for PM1 and PM2.5. This case is plotted in Figure 7 for PM2.5 fraction. Therefore, our data shows that equation (2) can be very useful to derive ground measurements from columnar retrievals, only if the mixing layer assumptions apply.

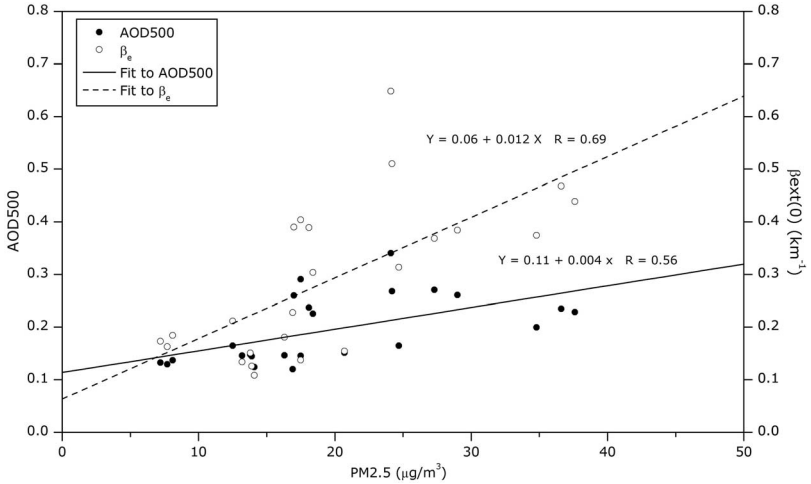

Figure 7. Scatterplots of PM2.5 levels with AOD at 500 nm (black dots and continuous line) and derived aerosol extinction coefficient (β_e) (white dots and dashed line) during days 28 June to 2 July. Points represent hourly averages.

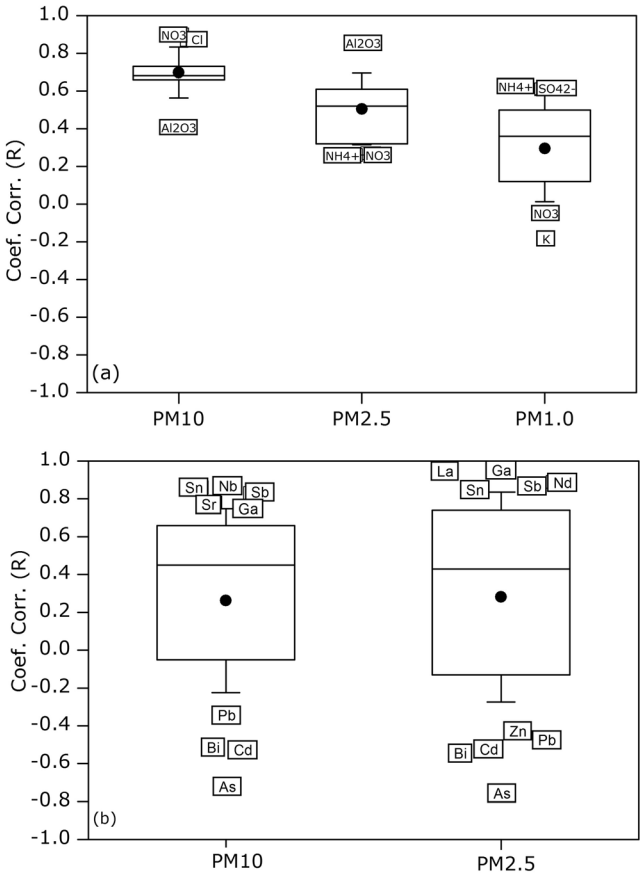

Figure 8. Statistical box diagram representing the correlation coefficients obtained for the (a) major chemical species in the three PM fractions and AOD and (b) minor chemical species in the PM10 and PM2.5 fractions.

3.5. Relationship Between Chemical Species and Columnar AOD

[44] The AOD has been also correlated with the concentration of the chemical species for the three PM fractions, separated in three different sets: (1) major species (Al_2O_3, Ca, Fe, K, Na, Mg, SO_4^{2-}, NO_3^-, Cl^-, NH_4^+), (2) trace components (Li, P, TI, V, Cr, Mn, Cu, Zn, Ga, As, Se, Rb, Sr, Nb, Cd, Sn, Sb, Ba, La, Ce, Nd, Pb and Bi) and (3) combination of different species in order to describe *crustal* particles, *secondary inorganic aerosols* (SIA), *carbonaceous species* (OM + EC) and *marine* particles (related to Na and Cl; however, due to uncertainties on Cl determination and its association with other species, we have only considered Na for marine aerosols). The proportion of non-determinate particulate mass (mostly related to water) was also included in the last group.

[45] To better visualize the correlation coefficients we have represented them statistically in Figure 8 as a box plot. In the box diagram, the solid dot represents the mean value of the sample, the box limits are percentiles U25 and U75, the box division is percentile U50 (median) and the bars represent the mean +/− the standard deviation. In the box plot we have highlighted the outlier species, it is, the chemical components whose correlation coefficient is higher/lower than the mean +/− the standard deviation. As the higher correlation coefficient outliers species correspond to those chemical species with a stronger correlation with AOD, we would expect them to be more responsible of the observed changes in the columnar aerosol burden.

[46] The correlation coefficients shown in Figure 8a are higher for PM10 and PM2.5 chemical levels (0.5–0.6) but lower for PM1 fraction. For PM10 fraction, NO_3^- and Cl^- reached maximum correlations (0.90 and 0.87 respectively). Both chemicals are related to particles of marine origin. Other marine tracers such as Na and Mg obtained high correlations too (0.72). Moreover, NO_3^- may represent in this case aged marine aerosols (the presence of $NaNO_3$ is dominant instead of NaCl [*Pey et al.*, 2008] and therefore it could explain that it turns to be less abundant and correlated (or even uncorrelated) in PM2.5 and PM1 fractions. Sulfate was abundant for the three fractions, but it did not dominate the AOD evolution.

[47] For the PM1 fraction, the better correlated species are NH_4^+ and SO_4^{2-}, reaching 0.63 in case of ammonia. These tracers increased during the pollution episode and dominate the columnar burden changes.

[48] Al and Ca can be considered tracers for mineral particles. The correlation coefficient for Al was 0.86 for PM2.5 and 0.41 for PM10. This difference in the correlation could be related to the local character of PM10 marine and mineral particles, but also to the stronger weight of the marine particles in the PM10 mode. It is also possible that marine particles are better distributed in the column and therefore more correlated to AOD.

[49] The box plot in Figure 8b represents the correlation analysis performed for the minor species. Concentration of these tracers is generally very low, even undetectable for PM1 fraction, so the analysis has been only performed for those metals with a minimum detection threshold for PM1 and PM2.5.

[50] Despite its low concentrations, we actually found that some tracers are very well correlated with the columnar AOD. Sn and Sb typically related to traffic [*Querol et al.*, 2007] and are well correlated in both PM10 and PM2.5 levels (0.86 and 0.83, respectively). Mineral tracers such as Li, Ga, Sr or Nb are also well correlated, with correlation coefficients between 0.66 (Li) and 0.87 (Ga) for PM10.

[51] On the other hand, other species also exhibit a strong anti-correlation. For example, Bi, Pb and As are industrial tracers from Huelva area. *Sánchez de la Campa et al.* [2007] registered their maximum concentrations when lower PM and AOD levels were measured, showing a marked anti – correlation with AOD (−0.72 for As).

[52] The third group of chemical species to be correlated with AOD is composed by combinations of individual species related to a particular origin, it is: crustal, SIA, carbon and marine. The resultant correlation coefficients have been

Table 5. Correlation Coefficients Obtained by Linear Regression of AOD500 Versus PM10, PM2.5 and PM1 for Crustal, SIA, OM + EC, Marine and Nondeterminate Components

Species	PM10	PM2.5	PM1
Crustal	0.55	0.80	0.37
CIS	0.84	0.71	0.61
OM + EC	0.56	0.54	0.11
Marine	0.72	0.55	0.50
Nondetermined	0.76	0.48	0.63

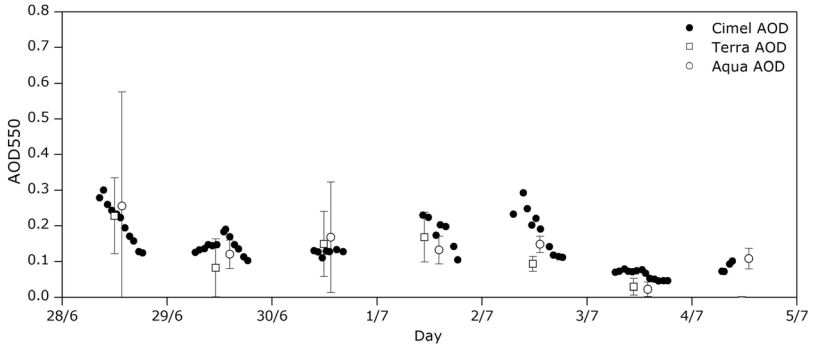

Figure 9. Compared temporal evolution of AOD at 550 nm retrieved by the Cimel sunphotometer and the MODIS sensor on Terra/Aqua platforms. The error bars represent the standard deviation of AOD in the selected area around El Arenosillo station.

presented in Table 5. Secondary components were the most abundant (24–39% mass for the three fractions) during the field campaign [*Pey et al.*, 2008] and so they are also well correlated for the three size fractions (0.61–0.84). These components are less related to local sources and therefore their distribution along the column could be more homogeneous, mainly for fractions PM1 and PM2.5. Organic matter and elemental carbon are the second most abundant species (20–25% mass for the three fractions) but in this case the correlation is the lowest, possibly due to a change on the pollution origin (carbon compounds decreased during the high PM episode).

[53] As expected from the analysis of individual chemicals, crustal tracers are best correlated for the PM2.5 fraction (0.80) and marine species are best correlated for the PM10 fraction (0.72) in spite of their low concentration during the campaign (4–13% for crustal, and 1–10% for marine). A nondeterminate fraction of mass was nonnegligible and it was best correlated in PM10 fraction. This fraction was mostly composed by water, associated to hydrophilic species such as coarse nitrate and sea spray present in PM10 fraction, but also to SIA components in PM1. Therefore, the high correlation found for PM10 could be also driven by the combination of water vapor and marine hydrophilic species; and for PM1, both SIA and water would drive the changes in particulate matter and on the columnar burden.

[54] A few authors have previously studied the relationship between the columnar extinction and the chemical analysis of ground PM samples at three fractions. *Slater et al.* [2004] analyzed 8 inorganic ions and carbon (EC and OC) in 24 h filters for PM10 and PM2.5. With a 96 days database they could trace two different distant source areas of pollution, characterized by a different dominance of sulfate and carbonaceous compounds. *Cheng et al.* [2008] correlated aerosol columnar properties with ground level concentrations of chemical species (20 trace elements and gases) analyzed in 24 h filters. In this case, the analysis was only performed for dust intrusion days, so the amount of particulate matter was consequently high. The correlation they found between crustal elements and columnar properties was considered to be good (0.6–0.8). Due to the high aerosol concentration suffered during intrusion days, the chemical analysis of trace elements was more accurate, and their correlations were more significant than ours.

3.6. Performance Assessment of the MODIS AOD Product

[55] In previous sections we have shown the good correlation existing between ground measurements of PM, columnar AOD, LIDAR vertical profiles and some chemical components related to aerosol origin. Even in a relatively clean environment such as El Arenosillo site, these techniques were able to describe similarly the same day to day variations.

[56] However, the most interesting and challenging application would consist on successfully correlating the ground level particulate matter levels and the remote sensing columnar retrievals. Hence, we have also obtained the MODIS AOD at 550 nm as a level 3 product (Collection 5.1) from both Terra

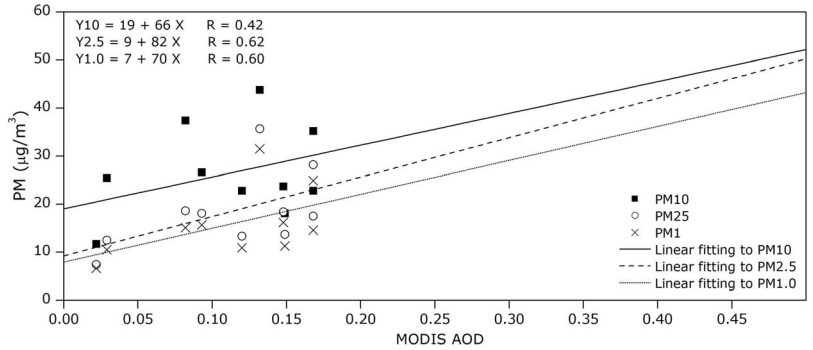

Figure 10. Scatterplot of ground PM levels and MOD/MYD aerosol optical depth at 550 nm. The linear fittings equations and correlation coefficients are also indicated in the plot.

and Aqua platforms. In Figure 9, MODIS and Cimel AOD at 550 nm has been plotted.

[57] Qualitatively, MODIS product is able to similarly reproduce the day to day variations of columnar AOD. In Figure 9, the error bars represent the standard deviation of the AOD sample within a selected 1° × 1° area centered on El Arenosillo station. Both Terra and Aqua overpasses have been used, and they are differently represented in the graph.

[58] In Figure 10 we have plotted the three ground level PM cuts against the MODIS AOD retrieval. The results show an acceptable correlation, also dependent on the PM fraction. In agreement with previous sections, the PM10 gets the lowest correlation coefficient (0.42). In contrast, the PM2.5 and PM1 cuts have similar correlation coefficients of 0.62 and 0.60.

[59] Furthermore, the intercept of the linear fittings are close to zero for both PM2.5 and PM1 cuts (9 $\mu g/m^3$ and 7 $\mu g/m^3$ respectively), as compared to the PM10 cut (19 $\mu g/m^3$). In contrast to the correlation between Cimel AOD and PM, these positive intercepts would be originated by the increased uncertainties in the surface reflectance [*Chu et al.*, 2002] mainly in low burden conditions.

4. Conclusions

[60] In this study we have correlated aerosol measurements at ground level (particulate matter or PM, and concentration of chemical species) and in the whole atmospheric column (represented by the aerosol optical depth or AOD at 500 nm) during the DAMOCLES 2006 field campaign. This field campaign took place in El Arenosillo station (Huelva, Spain) in summer 2006. During this field campaign, three different phases were identified, based on the analysis of meteorological measurements and numerical simulations of the atmospheric conditions. The effect of these different conditions was evident in the variable properties of the atmospheric particles, and an episode of high pollution was consequently identified and characterized.

[61] To relate ground and columnar values, linear regressions were fitted to the data. In general, columnar AOD500 and ground level PM evolution agreed well, with correlation coefficients that ranged from 0.71 to 0.81 for PM10, PM2.5 and PM1, when spectrometer daily means were used. Best correlations were found for the lowest fractions. Differences PM10–PM2.5 and PM2.5–PM1 were also correlated with AOD500. The use of these fractions allows us to isolate the different modes in the size distribution. The results show that PM1 fraction drives the correlation with AOD. The AOD was shown not to be very sensitive to variations on PM10.

[62] The effect of the vertical structure of the aerosol layers has been taken into account by retrieving the mixing layer height from the LIDAR profiles. From the AOD and the MLH, an effective extinction coefficient has been estimated. This extinction coefficient has been correlated with PM levels instead of AOD. Using the extinction coefficient does not improve the global results significantly, although they can introduce a significant correction if introduced on cases where no elevated layers exist and the mixing layer is well mixed.

[63] Level 3 MODIS aerosol optical depth from Collection 5.1 has been also compared to Cimel retrievals and correlated to PM cuts. The correlation was higher for PM2.5 and PM1 cut sizes (R = 0.60–0.62).

[64] Finally, the relationship of AOD with a series of chemical species has been also analyzed. The secondary components were the most abundant and were also well correlated in the three size fractions. Traffic (Sn, Sb) and mineral (Li, Ga, Sr or Nb) tracers were found to be also well correlated in PM10 and PM2.5. For PM10 fraction, chemical species related to marine origin were the best correlated (correlation coefficients of 0.87 and 0.90 for Cl^- and NO_3^-).

[65] **Acknowledgments.** We would like to thank RIMA network for the use of the CIMEL data and calibration. Analyses used in this paper were produced with the Giovanni online data system, developed and maintained by the NASA GES DISC. We also acknowledge the MODIS mission scientists and associated NASA personnel for the production of the data used in this research effort. The study was supported by the Acción Especial CGL-2006-27108-E/CLI of the Spanish Ministry of Education and Science in the framework of the DAMOCLES Aerosol Scientific Thematic Network. The Solar Radiation Group was supported by project CGL2009–07790 of the Spanish Ministry of Science and Innovation (MICINN), and the project PROMETEO-2010-064 of the Valencia Autonomous Government. MICINN is also acknowledged for its support through the Complementary Actions CGL2008-01330-E/CLI and CGL2009-08031-E/CLI.

References

Acker, J. G., and G. Leptoukh (2007), Online analysis enhances use of NASA Earth science data, *Eos Trans. AGU*, *88*(2), 14–17, doi:10.1029/2007EO020003.

Alastuey, A., X. Querol, F. Plana, M. Viana, C. R. Ruiz, A. Sánchez de la Campa, J. de la Rosa, E. Mantilla, and S. García dos Santos (2006), Identification and chemical characterisation of industrial PM sources in SW Spain, *J. Air Waste Manage.*, *56*, 993–1006.

Alföldy, B., J. Osán, Z. Tóth, S. Török, A. Harbusch, C. Jahn, S. Emeis, and K. Schäfer (2007), Aerosol optical depth, aerosol composition and air pollution during summer and winter conditions in Budapest, *Sci. Total Environ.*, *383*, 141–163, doi:10.1016/j.scitotenv.2007.04.037.

Boyouk, N., J. F. Leon, H. Delbarre, T. Podvin, and C. Deroo (2010), Impact of the mixing boundary layer on the relationship between $PM_{2.5}$ and aerosol optical thickness, *Atmos. Environ.*, *44*, 271–277, doi:10.1016/j.atmosenv.2009.06.053.

Cachorro, V. E., et al. (2007), Iberian Network for Photometric Aerosol Measurements, paper presented at the 34th Annual European Meeting on Atmospheric Studies by Optical Methods, Univ. of Valladolid, Andenes, Norway.

Cheng, T., R. Zhang, Z. Han, and W. Fang (2008), Relationship between ground-based particle component and column aerosol optical property in dusty days over Beijing, *Geophys. Res. Lett.*, *35*, L20808, doi:10.1029/2008GL035284.

Chu, D. A., Y. J. Kaufman, C. Ichoku, L. A. Remer, D. Tanré, and B. N. Holben (2002), Validation of MODIS aerosol optical depth retrieval over land, *Geophys. Res. Lett.*, *29*(12), 8007, doi:10.1029/2001GL013205.

Chu, D. A., Y. J. Kaufman, G. Zibordi, J. D. Chern, J. Mao, C. Li, and B. N. Holben (2003), Global monitoring of air pollution over land from the Earth Observing System-Terra Moderate resolution imaging spectroradiometer (MODIS), *J. Geophys. Res.*, *108*(D21), 4661, doi:10.1029/2002JD003179.

Corbin, K. C., S. M. Kreidenweis, and T. H. Vonder Haar (2002), Comparison of aerosol properties derived from Sun photometer data and ground-based chemical measurements, *Geophys. Res. Lett.*, *29*(10), 1363, doi:10.1029/2001GL014105.

Córdoba-Jabonero, C., et al. (2011), Synergetic monitoring of Saharan dust plumes and potential impact on surface: A case study of dust transport from Canary Islands to Iberian Peninsula, *Atmos. Chem. Phys.*, *11*, 3067–3091, doi:10.5194/acp-11-3067-2011.

Das, N., S. S. Baral, S. K. Sahoo, R. K. Mohapatra, T. S. Ramulu, S. N. Das, and G. R. Chaudury (2009), Aerosol physical characteristics at Bhubaneswar, East coast of India, *Atmos. Res.*, *93*, 897–901, doi:10.1016/j.atmosres.2009.04.013.

Estellés, V., et al. (2006), Intercomparison of spectroradiometers and sunphotometers for the determination of the aerosol optical depth during the VELETA2002 field campaign, *J. Geophys. Res.*, *111*, D17207, doi:10.1029/2005JD006047.

Estellés, V., M. Campanelli, T. J. Smyth, M. P. Utrillas, and J. A. Martínez-Lozano (2010), AERONET and EuroSkyrad (ESR) aerosol optical depth

intercomparison on CIMEL CE318 and Prede POM01 radiometers, *Proc. SPIE Int. Soc. Opt. Eng.*, *7827*, 78270Y, doi:10.1117/12.865039.

Estellés, V., M. Campanelli, M. P. Utrillas, F. Expósito, and J. A. Martínez-Lozano (2011), Comparison of AERONET and SKYRAD4.2 inversion products retrieved from a Cimel CE318 sunphotometer, *Atmos. Meas. Tech. Discuss.*, *4*(6), 6883–6913, doi:10.5194/amtd-4-6883-2011.

European Parliament (2008), Directive 2008/50/EC of the European Parliament and of the Council of 21 May 2008 on ambient air quality and cleaner air for Europe (2008), *Off. J. Eur. Union*, *11.6.2008*, L152/1–L152/44.

Fernald, F. G. (1984), Analysis of atmospheric lidar observations: Some comments, *Appl. Opt.*, *23*, 652–653, doi:10.1364/AO.23.000652.

Guo, J.-P., et al. (2009), Correlation between PM concentrations and aerosol optical depth in eastern China, *Atmos. Environ.*, *43*, 5876–5886, doi:10.1016/j.atmosenv.2009.08.026.

Hutchison, K. D., S. Smith, and S. J. Faruqui (2005), Correlating MODIS aerosol optical thickness data with ground-based $PM_{2.5}$ observations across Texas for use in a real-time air quality prediction system, *Atmos. Environ.*, *39*, 7190–7203, doi:10.1016/j.atmosenv.2005.08.036.

Kaskaoutis, D. G., H. D. Kambezidis, P. T. Nastos, and P. G. Kosmopoulos (2008), Study on an intense dust storm over Greece, *Atmos. Environ.*, *42*, 6884–6896, doi:10.1016/j.atmosenv.2008.05.017.

Kim, J. E., S. Y. Ryu, Z. He, and Y. J. Kim (2006), Spectral aerosol optical depth variation with different types of aerosol at Gwangju, Korea, *J. Atmos. Sol. Terr. Phys.*, *68*, 1609–1621, doi:10.1016/j.jastp.2006.05.008.

Klett, J. D. (1985), Lidar inversion with variable backscatter/extinction ratios, *Appl. Opt.*, *24*, 1638–1643, doi:10.1364/AO.24.001638.

Koelemeijer, R. B. A., C. D. Homan, and J. Matthijsen (2006), Comparison of spatial and temporal variations of aerosol optical thickness and particulate matter over Europe, *Atmos. Environ.*, *40*, 5304–5315, doi:10.1016/j.atmosenv.2006.04.044.

Lipfert, F. W., J. Zhang, and R. E. Wyzga (2000), Infant mortality and air pollution: A comprehensive analysis of U.S. data for 1990, *J. Air Waste Manage. Assoc.*, *50*, 1350–1366.

Martínez-Lozano, J. A., L. Alados-Arboledas, B. A. De la Morena, V. Estellés, F. J. Exposito, J. Pey, M. Sicard, and M. Sorribas (2007), Intercomparison of instrumentation for atmospheric aerosol measurements: DAMOCLES campaign, paper presented at European Aerosol Conference 2007, Eur. Aerosol Soc., Manchester, U. K.

Mészáros, E. (1999), *Fundamentals of Atmospheric Aerosol Chemistry*, Akadémiai, Kiado, Hungary.

Mukai, S., I. Sano, M. Sato, and B. N. Holben (2006), Aerosol properties and air pollutants over an urban area, *Atmos. Res.*, *82*, 643–651, doi:10.1016/j.atmosres.2006.02.020.

Mukai, S., I. Sano, A. Nishimori, M. Sato, Y. Okada, and B. N. Holben (2007), A comparison of aerosol properties with air pollutants, *Adv. Space Res.*, *39*, 32–35, doi:10.1016/j.asr.2006.02.033.

Pey, J., et al. (2008), Characterization of a long range transport pollution episode affecting PM in SW Spain, *J. Environ. Monit.*, *10*(10), 1158–1171, doi:10.1039/b809001g.

Pielke, R. A., et al. (1992), A comprehensive meteorological modeling system-RAMS, *Meteorol. Atmos. Phys.*, *49*, 69–91, doi:10.1007/BF01025401.

Pio, C., L. M. Castro, and M. Ramos (1994), Differentiated determination of organic and elemental carbon in atmospheric aerosol behaviour of atmospheric pollutants, in *Physico-chemical Behaviour of Atmospheric Pollutants*, edited by G. Angeletti and G. Restelli, *Rep. EUR 15609/1 EN*, vol. 1, pp. 706–711, Eur. Comm., Brussels.

Pope, A., R. T. Burnett, M. J. Thun, E. E. Calle, D. Krewski, K. Ito, and G. D. Thurston (2002), Lung cancer, cardiopulmonary mortality, and long term exposure to fine particulate air pollution, *J. Am. Med. Assoc.*, *287*, 1132–1141, doi:10.1001/jama.287.9.1132.

Querol, X., et al. (2007), Source origin of trace elements in PM from regional background, urban and industrial sites of Spain, *Atmos. Environ.*, *41*, 7219–7231, doi:10.1016/j.atmosenv.2007.05.022.

Ramachandran, S. (2005), $PM_{2.5}$ mass concentrations in comparison with aerosol optical depth over the Arabian Sea and Indian Ocean during winter monsoon, *Atmos. Environ.*, *39*, 1879–1890, doi:10.1016/j.atmosenv.2004.12.003.

Raut, J.-C., and P. Chazette (2009), Assessment of vertically resolved PM_{10} from mobile lidar observations, *Atmos. Chem. Phys.*, *9*, 8617–8638, doi:10.5194/acp-9-8617-2009.

Reba, M. N. M. (2010), Data processing and inversion interfacing the UPC elastic-Raman lidar system, Ph.D. thesis, Dep. of Signal Theory and Commun., Univ. Politécnica de Catalunya, Barcelona, Spain.

Rocadenbosch, F., M. Sicard, A. Comerón, J. M. Baldasano, A. Rodríguez, R. Agishev, C. Muñoz, M. A. López, and D. García-Vizcaino (2002), The UPC scanning Raman lidar: An engineering overview, in *21st International Laser Radar Conference*, vol. 1, edited by L. Bissonette, G. Roy, and G. Vallée, pp. 69–70, Defense Res. and Dev.–Valcartier, Quebec, Que., Canada.

Sánchez de la Campa, A., J. de la Rosa, X. Querol, A. Alastuey, and E. Mantilla (2007), Geochemistry and origin of PM10 at rural background site in south-western Spain, *Environ. Res.*, *103*, 305–316.

Sasano, Y., and H. Nakane (1984), Significance of the extinction/backscatter ratio and the boundary value term in the solution for the two-component lidar equation, *Appl. Opt.*, *23*, 11-1–11-13, doi:10.1364/AO.23.0011_1.

Schaap, M., A. Apitulry, R. M. A. Timmermans, R. B. A. Koelemeijer, and G. de Leeuw (2009), Exploring the relation between aerosol optical depth and $PM_{2.5}$ at Cabauw, The Netherlands, *Atmos. Chem. Phys.*, *9*, 909–925, doi:10.5194/acp-9-909-2009.

Schäfer, K., A. Harbusch, S. Emeis, P. Koepke, and M. Wiegner (2008), Correlation of aerosol mass near the ground with aerosol optical depth during two seasons in Munich, *Atmos. Environ.*, *42*, 4036–4046, doi:10.1016/j.atmosenv.2008.01.060.

Sicard, M., C. Pérez, F. Rocadenbosch, J. M. Baldasano, and D. García-Vizcaino (2006), Mixed-layer depth determination in the Barcelona coastal area from regular lidar measurements: Methods, results and limitations, *Boundary Layer Meteorol.*, *119*, 135–157, doi:10.1007/s10546-005-9005-9.

Sicard, M., et al. (2009), Aerosol Lidar intercomparison in the framework of SPALINET–The Spanish Lidar Network: Methodology and results, *IEEE Trans. Geosci. Remote Sens.*, *47*(10), 3547–3559, doi:10.1109/TGRS.2009.2021525.

Slater, J. F., J. E. Dibb, J. W. Campbell, and T. S. Moore (2004), Physical and chemical properties of surface and column aerosols at a rural New England site during MODIS overpass, *Remote Sens. Environ.*, *92*, 173–180, doi:10.1016/j.rse.2004.05.011.

Smirnov, A., B. N. Holben, D. Savoie, J. M. Prospero, Y. J. Kaufman, D. Tanre, T. F. Eck, and I. Slutsker (2000), Relationship between column aerosol optical thickness and in situ ground based dust concentrations over Barbados, *Geophys. Res. Lett.*, *27*(11), 1643–1646, doi:10.1029/1999GL011336.

Sorribas, M. (2008), Medida y Caracterización del Aerosol Atmosférico en un Ambiente Rural y Costero del Suroeste de Europa. La distribución Numérica de Tamaños en el Rango Sub-micrométrico (Measurements and characterization of atmospheric aerosol in a rural and coastal environment. Sub-micron particle number size distribution in Southwestern Europe), PhD thesis, 350 pp., Univ. of Valladolid, Valladolid, Spain. [Available at http://sites.google.com/site/marsorribas/.]

Tian, J., and D. Chen (2010), A semi-empirical model for predicting hourly ground-level fine particulate matter ($PM_{2.5}$) concentration in southern Ontario from satellite remote sensing and ground-based meteorological measurements, *Remote Sens. Environ.*, *114*, 221–229, doi:10.1016/j.rse.2009.09.011.

Tremback, C. J., W. A. Lyons, W. P. Thorson, and R. L. Walko (1993), An emergency response and local weather forecasting software system, in *Proceedings of the 20th International Technical Meetings of NATO/CCMS on Air Pollution and its Application*, pp. 423–429, Plenum, New York.

van de Kassteele, J., R. B. A. Koelemeijer, A. L. M. Dekkerrs, M. Schaap, C. D. Homan, and A. Stein (2006), Statistical mapping of PM_{10} concentrations over Western Europe using secondary information from dispersion modelling and MODIS satellite observations, *Stochastic Environ. Res. Risk Assess.*, *21*(2), 183–194, doi:10.1007/s00477-006-0055-4.

van Donkelaar, A., R. V. Martin, and R. J. Park (2006), Estimating ground level $PM_{2.5}$ with aerosol optical depth determined from satellite remote sensing, *J. Geophys. Res.*, *111*, D21201, doi:10.1029/2005JD006996.

Veefkind, J. P., J. C. H. van der Hage, and H. M. ten Brink (1996), Nephelometer derived and directly measured aerosol optical depth of the atmospheric boundary layer, *Atmos. Res.*, *41*, 217–228, doi:10.1016/0169-8095(96)00011-7.

Wang, J., and S. A. Christopher (2003), Intercomparison between satellite-derived aerosol optical thickness and $PM_{2.5}$ mass: Implications for air quality studies, *Geophys. Res. Lett.*, *30*(21), 2095, doi:10.1029/2003GL018174.

Wilson, W. E. (1998), Fine and coarse particles: Chemical and physical properties important for the standard-setting process, in *Air Pollution in the 21st Century: Priority Issues and Policy*, edited by T. Schneider, pp. 87–115, Elsevier, Amsterdam.

World Health Organization (1999), Air quality guidelines for Europe, *Eur. Ser. 91*, 288 pp., Copenhagen.

Xia, X. A., H. B. Chen, P. C. Wang, W. X. Zhang, P. Goloub, B. Chatenet, T. F. Eck, and B. N. Holben (2006), Variation of column-integrated aerosol properties in a Chinese urban region, *J. Geophys. Res.*, *111*, D05204, doi:10.1029/2005JD006203.

Zhang, L., X. Cao, J. Bao, B. Zhou, J. Huang, J. Shi, and J. Bi (2010), A case study of dust aerosol radiative properties over Lanzhou, China, *Atmos. Chem. Phys. Discuss.*, *10*, 2889–2914, doi:10.5194/acpd-10-2889-2010.

A. Alastuey, J. Pey, and X. Querol, Instituto de Diagnóstico Ambiental y Estudios del Agua, CSIC, c/ Lluís Sole i Sabarís s/n, E-08028 Barcelona, Spain.

V. Estellés, A. R. Esteve, J. A. Martínez-Lozano, and M. P. Utrillas, Grupo de Radiación Solar, Departamento Física de la Tierra y Termodinámica, Universidad de Valencia, Dr. Moliner 50, E-46100 Burjassot, Valencia, Spain. (victor.estelles@uv.es)

G. Gangoiti, Departamento de Ingeniería Química y del Medio Ambiente, Universidad del País Vasco, Alameda de Urquijo s/n, E-48013 Bilbao, Spain.

F. Rocadenbosch and M. Sicard, Department of Signal Theory and Communications, Universitat Politècnica de Catalunya, c/ Jordi Girona, 1-3, Edif. D4-010, E-08034 Barcelona, Spain.

M. Sorribas, Estación de Sondeos Atmosféricos "El Arenosillo," INTA, Ctra. Huelva – Matalascañas, km 33, E-21130 Huelva, Spain.